Interfacial Phenomena and Heat Transfer, 1 (3): 273–287 (2013)

EFFECTS OF PSEUDOPLASTICITY ON SPREAD AND RECOIL DYNAMICS OF AQUEOUS POLYMERIC SOLUTION DROPLETS ON SOLID SURFACES

Vishaul Ravi, Milind A. Jog,* & Raj M. Manglik

Thermal-Fluids and Thermal Processing Laboratory, Department of Mechanical and Materials Engineering, University of Cincinnati, Cincinnati, Ohio, 45221-0072, USA

*Address all correspondence to Milind A. Jog, E-mail: Milind.Jog@uc.edu

The postimpact spreading and recoil behavior of millimeter-size liquid droplets of pure water, water–glycerol solution, and non-Newtonian aqueous solutions of medium-grade hydroxyl ethyl cellulose (HEC 250 MR) on dry horizontal hydrophobic (Teflon) and hydrophilic (glass) substrates is presented. The drop spread–recoil dynamics are captured using a high-speed high-resolution digital video recording and image processing. The non-Newtonian effects of aqueous polymeric solutions on postimpact spreading are contrasted with those for a water–glycerol solution with identical surface tension and zero-shear rate viscosity. For a broad range of drop Weber numbers ($20 \leq We \leq 200$), dynamic visualized records of impact, spreading, and recoil are presented along with their measured temporal variations in drop-diameter-scaled spread and film height. The shear-rate-dependent viscosity of the polymer solution is found to give rise to highly complex spread–recoil dynamics compared to Newtonian liquids. During initial spread, because the shear rate tends to be high, shear-thinning or pseudoplasticity effects manifest in polymer solution drops to alter their spread dynamics. Contrarily, during recoil their higher low-shear apparent viscosity tends to retard recoil and dampen shape oscillations. Shear-rate-dependent non-Newtonian behavior is further seen at low We (low shear rate during spreading), where the maximum spread of HEC solution droplets is comparable to that of high-viscosity water–glycerol solution, whereas at high We (high shear rate during spreading), their maximum spreads are closer to those of low-viscosity water droplets.

KEY WORDS: *spray drop-coating, non-Newtonian drops, drop-spread film*

1. INTRODUCTION

The process of liquid droplet impact and spreading on dry solid surfaces forms a critical part of many practical applications, including spray cooling, spray coating, crop spraying, drug delivery, DNA sampling, and inkjet printing, among many others. Often the fluid in these applications tends to display non-Newtonian behavior. Characterizing the fundamental dynamics of spreading of Newtonian liquid droplets has received much attention in a large body of the literature (Chandra and Avedisian, 1991; Asai et al., 1993; Pasandideh-Fard et al., 1996; Mao et al., 1997; Sadhal et al., 1997; Rioboo et al., 2001; ikalo et al., 2002; Roisman et al., 2002; Ukiwe and Kwok, 2005; Šikalo and Ganiç, 2006; Yarin, 2006; Gatne et al., 2007; Sanjeev et al., 2008; Gatne et al., 2009; Ravi et al., 2010), and so also have been the efforts to delineate the drop-surface interactions in a variety of applications that range from macroscale processes to microscale devices (Jones, 1971; Madejski, 1976; Collings et al., 1990; Castrejón-Pita et al., 2011; Yang et al., 2012, 2013; as well as several others). For velocities below the splashing limit, the drop tends to spread on the surface to form a thin lamella. The surface tension force causes the liquid to retract in a column, which then falls back and again spreads on the surface. Such spread–recoil oscillations continue with decaying amplitude until viscous dissipation causes the droplet to reach a steady shape. The effects of impact velocity, drop size, liquid properties (density, surface tension, and viscosity), and surface wettability on the spread dynamics have been discussed extensively in the literature (see, for example, Sadhal et al., 1997; Šikalo et al., 2002; Yarin, 2006; Manglik et al., 2013).

2152–5080/13/$35.00

NOMENCLATURE

C	concentration (mol/cc)	We	Weber number ($\rho v^2 d/\sigma$) (–)
Ca	capillary number ($\mu v/\sigma$) (–)	β	spread factor (D/d) (–)
d	drop diameter (m)	$\beta_{\max}$	maximum spread factor ($D_{\max}/d$) (–)
D	drop spread (m)	γ	shear rate (1/s)
h	height of the liquid layer (m)	μ	viscosity (mPa s)
K	flow consistency index, Eq. (1) (Pa s^n)	μ_o	zero-shear-rate viscosity (mPa s)
n	flow behavior index, Eq. (1) (–)	ρ	density (kg/m^3)
v	drop-impact velocity (m/s)	σ	surface tension of the fluid (mN/m)
Oh	Ohnesorge number ($\mu/\sqrt{\rho\sigma d}$) (–)	τ	surface age (s)

In characterizing the spreading process, the temporal variations of instantaneous drop spread D and its height h are usually normalized by the prior to impact drop diameter d (see Fig. 1) and represented by their respective dimensionless spread factor ($\beta = D/d$) and flatness factor (h/d). A major thrust of much of the reported work has been to determine the maximum spread of the drop on different hydrophilic and hydrophobic substrates. Several correlations for the maximum spread have been developed by applying the principle of conservation of energy between the point of maximum spread and the instant just prior to impact (Jones, 1971; Madejski, 1976; Collings et al., 1990; Chandra and Avedisian, 1991; Asai et al., 1993; Pasandideh-Fard et al., 1996; Mao et al., 1997; Rioboo et al., 2001; Šikalo et al., 2002; Ukiwe and Kwok, 2005). While the correlations work reasonably for water on hydrophilic substrates, their predictions differ considerably from experimental measurements for other liquid–substrate combinations (Gatne et al., 2006, 2009).

Few attempts have been made to model the postimpact transient drop spread–recoil–oscillation to equilibrium behavior. A notable exception is a recent paper by Manglik et al. (2013), where it has been demonstrated that low-Weber-number drop dynamics on a hydrophobic substrate can be modeled as a harmonic mass-spring-damper system. With this innovative approach, drop dynamics for liquids covering a wide range of viscosities and surface tension coefficients (Ohnesorge and capillary numbers varying by 3 orders of magnitude ($0.002 \leq \text{Oh} \leq 1.57$; $0.007 \leq \text{Ca} \leq 7.59$) were correlated. The predictions of spread factor and flatness factor variations by the damped harmonic model agreed well with the experimental measurements. It was further shown that the frequency of oscillation for the spread factor is different from that for the flatness factor due to the contact angle hysteresis.

While non-Newtonian liquids are used in a number of spray coating (paint, pharmaceutical media, pesticides) and clinical applications, relatively few investigations of drop spread–recoil dynamics have been carried out with such liquids. Moreover, these studies have considerable disagreement on the extent of effects of the non-Newtonian character of the liquid on spread dynamics. For example, wetting kinetics of aqueous solutions of polymer droplets

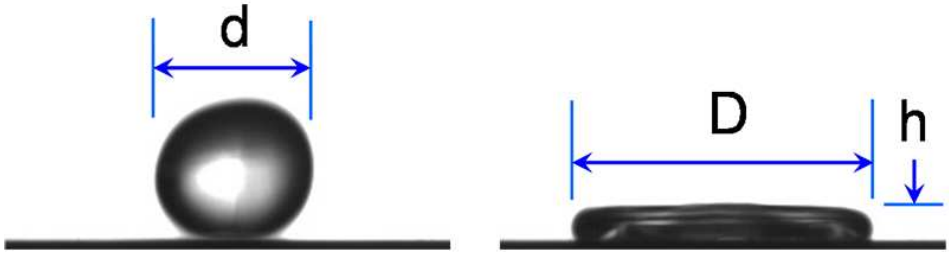

FIG. 1: Geometrical attributes of a droplet to characterize its spread and film height on a solid substrate.

was investigated by Schonhorn et al. (1966). They conducted their experiments with polymer melts on a low-energy surface (Teflon) and a high-energy surface (mica). In this work, they did not find any effect that could be ascribed to the non-Newtonian behavior of the polymer solutions on the drop wetting kinetics. This observation corroborates those reported by Nieh et al. (1996), Carre and Eustache (2000), and Neogi and Ybarra (2001), who found that pseudoplasticity or shear-thinning effects of the test solution did not significantly change the postimpact droplet behavior. However, contrasting from these results, Bergeron et al. (2000), Rafai et al. (2004), and Bartolo et al. (2007), for instance, show that droplets of shear-thinning polymeric solutions exhibit weaker recoil compared to a drop of a Newtonian fluid having the same zero-shear-rate viscosity and that the spread–recoil dynamics is significantly altered by non-Newtonian rheology. For many polymeric solutions, the apparent viscosity change with shear rate is nonuniform, where at very low shear rates the apparent viscosity is nearly constant (or has a Newtonian behavior), followed by a monotonic drop in apparent viscosity with increasing shear rate (shear-thinning or pseudoplastic behavior) (for example, see Bird et al., 1987; Bhatia et al., 2011). It is therefore quite possible that the differences in observations of the effects of non-Newtonian behavior on drop spread–recoil dynamics as reported in the literature may perhaps be related to the range of shear rates present in each set of experiments.

In this paper, and to address the reported dichotomy of reported results, we have investigated the drop-spread dynamics of aqueous solutions of a medium grade of the polymer hydroxyl ethyl cellulose (HEC 250 MR) with two different concentrations. To change the shear rate during spreading, the experiments were conducted with varying drop-impact velocity, and the corresponding drop Weber number ranged from 20 to 200. The spatial and temporal variations of relative spread and drop-film thickness or height are characterized on both a hydrophobic (Teflon) and hydrophilic (glass) substrate. Furthermore, to distinguish non-Newtonian effects, the results of spreading and recoil for a polymeric solution concentration were compared with those for two different Newtonian liquids: (1) an aqueous glycerin solution that had the same surface tension and viscosity as the equilibrium surface tension and zero-shear-rate viscosity of the former, and (2) water, which represented the low-viscosity asymptote for the polymeric solutions.

2. EXPERIMENTAL METHOD AND MATERIALS

The experimental setup for capturing high-speed digital images and characterizing the near-impact to postimpact drop–substrate interactions is schematically shown in Fig. 2. A droplet was generated through a flat-tipped stainless steel capillary-tube hypodermic syringe needle having on inner orifice diameter of 1.19 mm. The droplet was allowed to grow until it detached from the tip and fell on the substrate due to gravity. The two substrates, a hydrophobic Teflon plate and a hydrophilic glass plate, were placed directly below the syringe-needle drop generator on a horizontally leveled table. It may be noted that the cleaning process of these substrates is very critical, because the surface wetting behavior is sensitive to impurities and roughness of the surface. Thus the substrates were first rinsed with distilled water and subsequently by ethanol and acetone, wiped clean with a low-lint wipe, and dried. The clean, dry substrates were then placed on the leveling table and checked for flatness and their horizontal orientation relative to the vertical line of the drop generator. The surface energy, which includes roughness effects that influence wettability of each of the two substrates employed in this study, was characterized by the static contact angle measurement for a water sessile drop. The sessile drop was maintained at a diameter less than the capillary length $(=\sqrt{\sigma/\rho g})$ of water, and the contact angle was measured with $\pm 0.5^\circ$ precision from a high-definition goniometer. For the glass and Teflon surfaces used in the experiments, the measure equilibrium contact angle values were 23.7° and 121°, respectively, and their repeatability was verified by several different measurements.

The phenomenon of droplet impact and spread–recoil is captured with a high-speed, high–pixel-resolution digital camera system (Hi-DCam II version 3.0; NAC Image Technology). The camera has an 8 × zoom lens which helps capture clear magnified images during the process. A focusing, single-ended daylight PAR (parabolic aluminized reflector) "cold" lighting system (ARRI, Inc.) along with a glossy white reflector was used for providing sharply contrasting and continuous lighting for capturing the drop-spread dynamics. There was no noticeable rise in the temperature of the substrates when they were exposed to this light source during the entire experimentation process. The digital video camera was aligned horizontally in line and in plane with the substrate to record the drop-impact and postimpact evolution images in real time. The frame rate of the camera was set at 2000 fps and a shutter speed of 1/4000, and sequential images of the impinging drop and its postimpact spread–recoil–oscillations behavior were

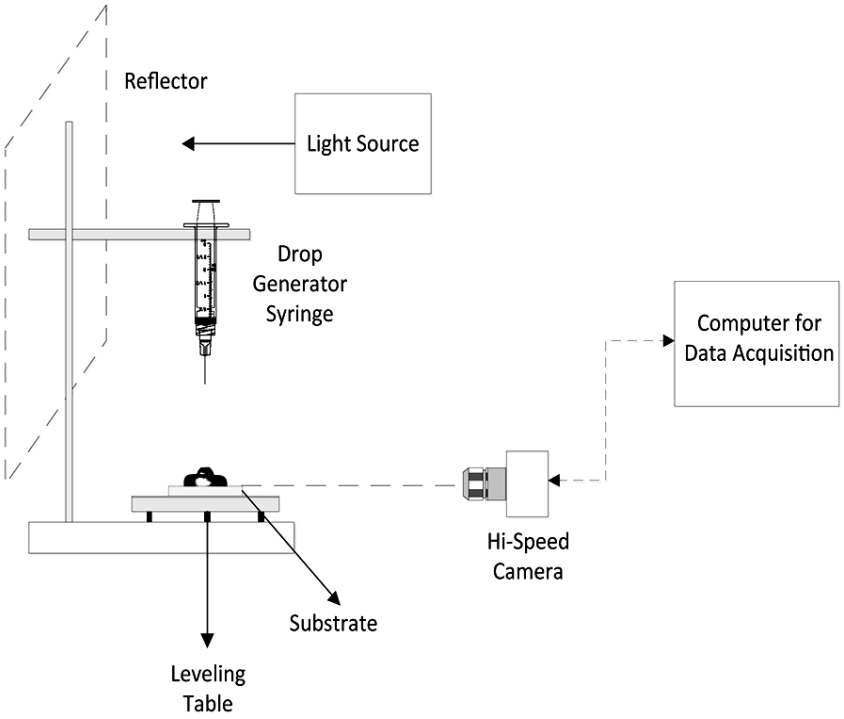

FIG. 2: Schematic of experimental data acquisition and analysis setup.

captured in real time high-resolution streaming video. The captured images were analyzed using an image-processing software (Image-Pro Plus 4.0 by Media Cybernetics), and for each drop-impact case (d, v, and We), several thousand short-timeframe images were analyzed to chart the variation of instantaneous drop spread and height with time. Moreover, because the size of the droplet produced from the needle orifice for each of the different liquids used in the experiments is governed by their respective properties (surface tension, viscosity, and density), the drop size may be different for each case and its value must be determined.

The drop mean diameter was thus determined by analyzing the image just prior to impact, and the droplet velocity was evaluated from a time series of images taken before impact. The actual droplet size, however, was obtained on an equivalent volume-average basis. For example, in determining the preimpact drop diameter, pixel area measurements were made on the drop-face image (digitally enhanced and enlarged) using four different images just before impact and their composite average calculated for the final value. In this manner any imprecision that may accrue due to slight noncircularity of drops is obviated and appropriately averaged. Moreover, drop spread was observed to be axisymmetric, with no splatter whatsoever for all the We conditions considered in these experiments. All measurements, both for the drop dynamics and fluid properties, were made for isothermal conditions of 23°C (see Table 1).

Besides distilled deionized water and a binary solution (75.46% glycerin–water), two solutions of HEC 250 MR in water in different concentrations were used in the experiments. The aqueous polymeric solutions were prepared by adding a specific amount of polymer powder to distilled deionized water. The powder was weighed using a precision weighing scale ($\pm$0.1 mg accuracy), and the solution was stirred at slow speed for a period of over 24 h using a magnetic stirrer to create homogenized polymeric test liquids. The polymer HEC 250 MR is both a surface-active reagent and a viscous additive, and hence the interfacial and rheological properties of its solutions were also measured.

The surface tension, or the gas–liquid interfacial tension, of all the liquids was measured using a twin-orifice, computerized surface tensiometer (model QC6000, CSC Scientific Company) that operates on the maximum bubble pressure method. Air at a constant pressure is bubbled into the test liquid through two probes with orifice diameters of 0.5 and 4.0 mm that are immersed into the test liquid. The difference in pressure between the two orifices, at the

TABLE 1: Properties of the aqueous polymeric solutions and Newtonian liquids at 23°C

	μ_o **(mPa s)**[1] $\pm$ **1.4%**	σ **(dyne/cm)**[1] $\pm$ **0.7%**	ρ **(kg/m^3)**[2]
HEC 250 MR (2.5×10^{-9} mol/cc)	5.25	66.9	1002.0
HEC 250 MR (6.0×10^{-9} mol/cc)	23.0	66.8	1004.5
Aqueous glycerin (75.46% glycerin)	23.0	66.8	1033.0
Water	1.0	72.5	1000.0

[1] As measured in this study.
[2] Based on water density, obtained at 23°C from NIST property database (REFPROP) for water and glycerin, and molecular mass of polymer concentration or volumetric ratio of binary solution.

time of bubble detachment at their tips, is proportional to the liquid surface tension. Also, the time interval between the newly formed interface and the point of bubble break-off at the orifice mouth, referred to as the surface age of the interface, gives the measurement of bubble growth time that corresponds to the dynamic surface tension value at a given operating bubble frequency. Thus, by altering the air-bubble frequencies through the probes, both equilibrium and dynamic surface tension can be measured. The equilibrium interfacial tension data were obtained with very low bubble frequencies at which static or unchanging conditions were obtained. Furthermore, the apparent viscosity of the polymeric solutions was measured using a rotating cup-and-cylinder rheometer (AR 2000, TA instruments) where the temperature control was maintained by the built-in Peltier heating system. This rheometer was used to measure the apparent viscosity at low shear rates ($\sim$10 to 400 s^{-1}), whereas for higher shear rates, several well-calibrated capillary-tube viscometers were used.

The maximum uncertainties in the measurements of the primary variables of this study were computed according to the single-sample error propagation method outlined by Moffat (1988) based on the precision of each measurement and instrumentation. The consequent uncertainty in the droplet diameter is $\pm$1.56% and that in drop velocity is $\pm$1.44%. Likewise, the maximum uncertainty in the calculated values of Weber number is $\pm$2.68%, and that in the spread diameter and height of the spreading droplet is $\pm$1.28% and $\pm$1.68%, respectively.

3. RESULTS AND DISCUSSION

The variations in the measured surface tension, or gas–liquid interfacial tension, with surface age for the HEC 250 MR aqueous solutions are shown in Fig. 3. For each of the two polymer concentrations (C = 6.0 $\times$ 10^{-9} and 2.5 $\times$ 10^{-9} mol/cc) of these solutions, the temporal variation of surface tension follows a similar trend. The interfacial tension is seen to decrease from that of the solvent (water, σ = 72.5 mN/m) to an asymptotic value of 66.8 mN/m in both cases. The majority of this change occurs over a time interval of about 200 ms, which is of the same order as the time scale for droplet spread–recoil dynamics.

The aqueous polymeric solutions also exhibit a shear-thinning behavior, as is seen in Fig. 4, where the apparent viscosity is graphed against the varying shear rate. This pseudoplastic viscous behavior can be represented by the following two asymptotic features: (1) as the shear rate $\gamma \rightarrow 0$, a Newtonian behavior is exhibited with a constant viscosity μ_o, and (2) at much higher shear rates the apparent viscosity is a decreasing function of shear rate, $\mu = \varphi(\gamma)$, to reflect the shear-thinning nature of the polymeric solution. This behavior can be mapped by the following modified power-law equation (Dunleavy and Middleman, 1966; Bhatia et al., 2011):

$$\mu_a = \mu_o \left[1 + (\mu_o/K)\,\gamma^{(1-n)}\right]^{-1} \tag{1}$$

Here, for the two HEC 250-MR solutions, K = 0.71 Pa $\cdot$ s^n and n = 0.51, for C = 6.0 $\times$ 10^{-9} mol/cc, and K = 0.08 Pa $\cdot$ s^n and n = 1.0, for C = 2.5 $\times$ 10^{-9} mol/cc. The measurements were repeatable and went to very low shear rates so as to validate both the constitutive equation given above and the zero-shear asymptote μ_o. Moreover, it may be noted that both the extent of pseudoplasticity (or shear thinning) and zero-shear viscosity are further seen to increase with polymer concentration.

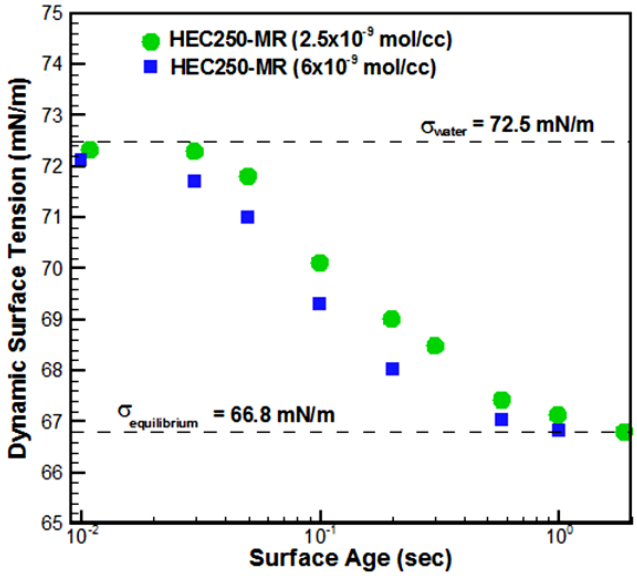

FIG. 3: Surface tension variation with surface age for HEC 250 MR solutions.

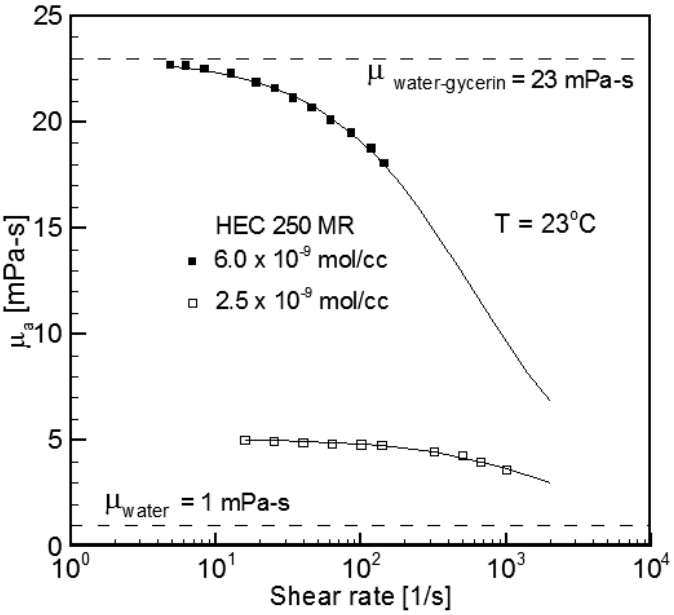

FIG. 4: Shear-dependent viscosity behavior for aqueous solutions of HEC 250 MR.

The high-speed images for spread of aqueous solutions of HEC MR 250 (C = 6.0 $\times$ 10^{-9} mol/cc) and glycerin (75.46% glycerin) along with pure water droplets on a glass substrate for We $\sim$ 20 are shown in Fig. 5. The corresponding temporal variations of spread factor and flatness factor are graphed in Figs. 6 and 7, respectively. The water droplet is seen to spread the most, followed sequentially by the polymer solution and aqueous glycerin droplet. Water undergoes the strongest recoil and its spread factor is seen to exhibit multiple oscillations. Considering the low viscos-

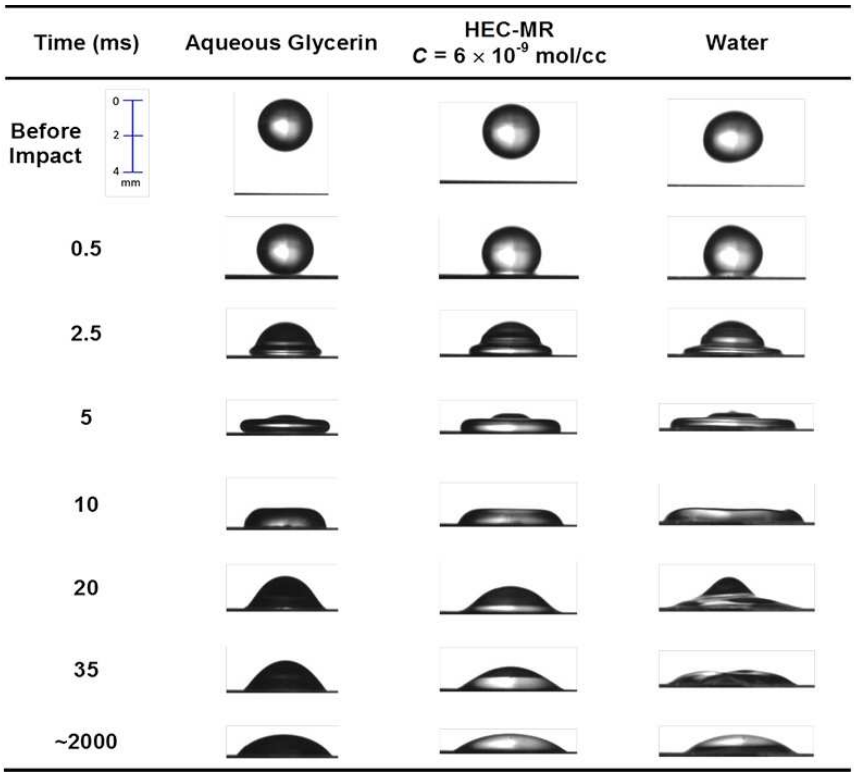

FIG. 5: High-speed photographs of drop spread on a glass substrate, We $\sim$ 20.

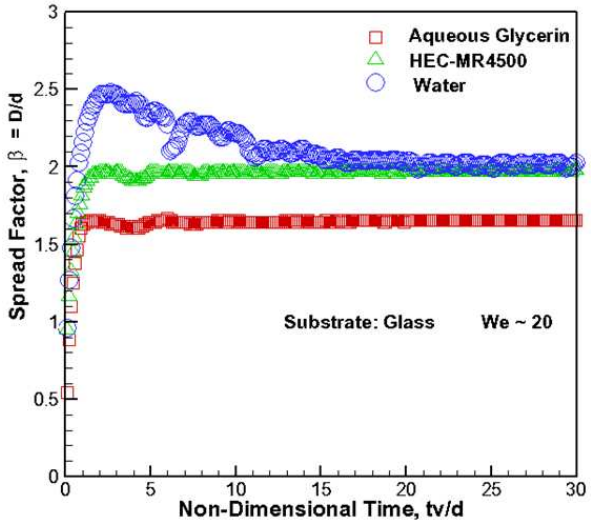

FIG. 6: Variation of the spread factor with dimensionless time. Glass substrate, We $\sim$ 20.

ity and high surface tension of water, this behavior is not surprising. Although water viscosity is lower than the other two liquids, each spread–recoil oscillation leads to significant viscous dissipation. Gatne et al. (2009) estimated that viscous dissipation scales as ($\mu v D^5/d^3$) and as such large spread (D/d) can significantly reduce the kinetic energy of

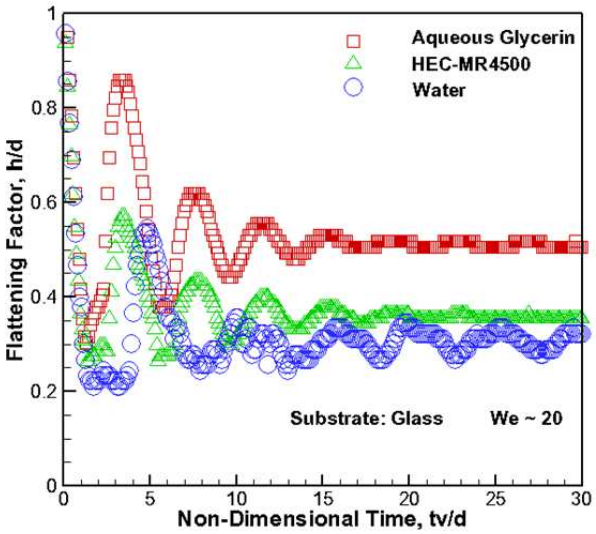

FIG. 7: Variation of flattening factor with nondimensional time. Glass substrate, We $\sim$ 20.

the drop and dampen the magnitude of spread–recoil oscillations. This is corroborated by the results in Fig. 7, where water flatness factor variation is much smaller than that for the more viscous counterparts. Furthermore, the high viscosity of aqueous glycerin solution resists initial spreading, and this produces a smaller maximum spread factor as compared to that for the other two liquids. The subsequent glycerin solution spread factor does not undergo oscillations but changes gradually. The initial kinetic energy is primarily dissipated through shape oscillations, causing large flatness factor variations with large damping. The behavior of a polymer solution droplet is more interesting, as it follows the low-viscosity water behavior in the early stages but adopts the high-viscosity aqueous glycerin droplet-spread dynamics during the later stages. The shear rate experienced by the polymeric solution droplet is high during initial spread and it gives rise to low apparent viscosity, thereby producing large spread similar to a water droplet. However, the recoil velocity is much smaller than the initial velocity. Correspondingly, the shear rate and apparent viscosity are high, and this produces small changes in spread on the substrate but large flatness factor variations similar to an aqueous glycerin droplet. These oscillations tend to damp out quickly but at a rate that is slightly slower than that seen in the behavior of the aqueous glycerin droplet.

The high-speed photographs of water, HEC MR 250 (C = 6.0 $\times$ 10^{-9} mol/cc) solution, and aqueous glycerin (75.46% glycerin) droplets are presented in Fig. 8 to depict the postimpact spread–recoil process at We $\sim$ 20 on a Teflon substrate. The corresponding spread factor and flatness factor variations are respectively graphed in Figs. 9 and 10. The maximum spread factor for water is less than the $\beta_{\max}$ value on a glass substrate. The water droplet produces strong recoil on the hydrophobic Teflon surface and undergoes large spread and flatness factor variations. The high-viscosity aqueous glycerin solution, on the other hand, has a maximum spread factor that is similar to that on a glass substrate but produces stronger recoil on the Teflon surface. This spread–recoil process leads to significant viscous dissipation, and the subsequent shape oscillations are smaller than those on glass and they damp out fairly quickly. The HEC MR 250 solution droplet initially spreads more than the aqueous glycerin droplet but less than the water droplet. Its lower surface tension and higher apparent viscosity compared to water causes weaker recoil. The shape oscillations are also damped much faster than what is seen in a water droplet.

Figures 11 and 12 depict the temporal variations of the dimensionless spread and height, respectively, for Weber number of 160 on a glass substrate. At this Weber number, all three liquid drops spread significantly more than what is observed at We $\sim$ 20. This is due to the higher impact velocity in the former case, and hence a correspondingly higher inertial force. Also, the polymeric solution droplet spreads appreciably more than the aqueous glycerin droplet. The shear rate experienced by the former is much higher than that at We $\sim$ 20, when the polymer solution essentially experiences a low apparent viscosity or shear-thinning effect during the initial spread. However, as the HEC MR droplet

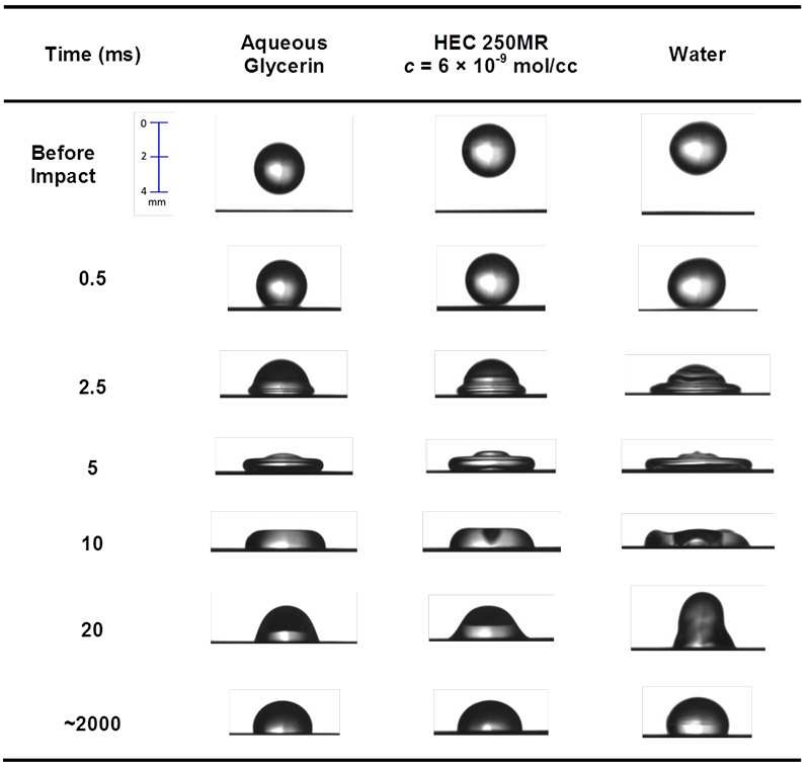

FIG. 8: High-speed photographs of drop spread on a Teflon substrate, We $\sim$ 20.

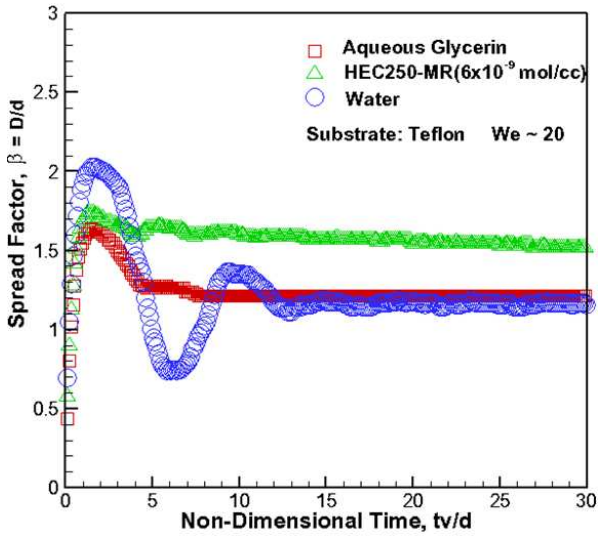

FIG. 9: Variation of the spread factor with nondimensional time. Teflon substrate, We $\sim$ 20.

reaches maximum spread, the shear rate decreases significantly and its much higher low-shear-rate apparent viscosity tends to slow the recoil process. The We $\sim$ 160 polymer solution droplet oscillates on the surface for a prolonged period of time compared to the aqueous glycerin droplet, which suggests that the viscous dissipation experienced by

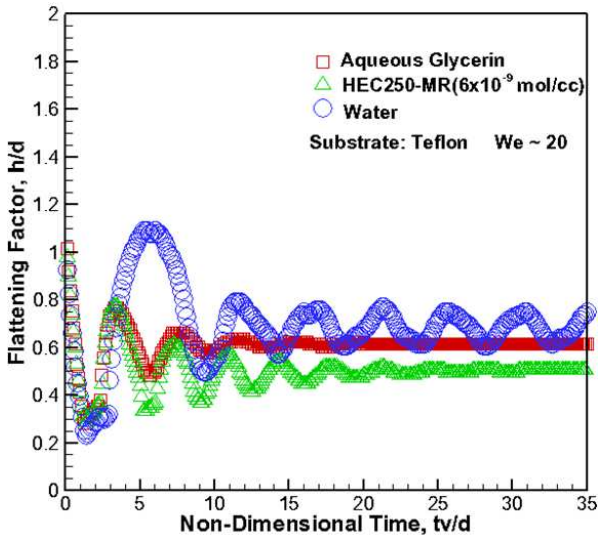

FIG. 10: Variation of the flattening factor with nondimensional time. Teflon substrate, We $\sim$ 20.

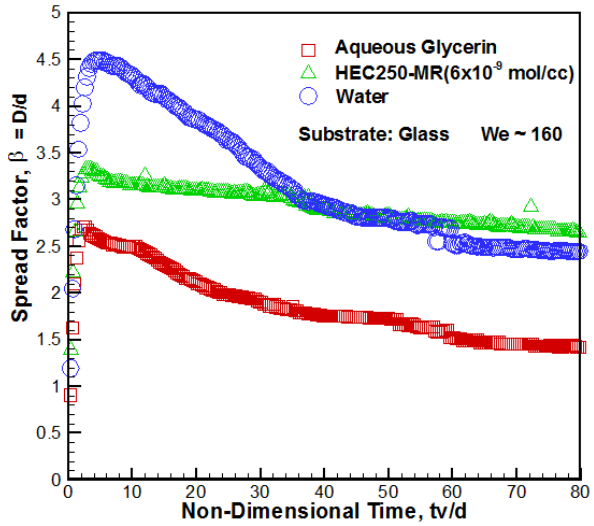

FIG. 11: Variation of spread factor with nondimensional time. Glass substrate, We $\sim$ 160.

the former is considerably lower. Interestingly, its equilibrium spread factor and flatness factor reach the values of that of aqueous glycerin after an extended time period ($\sim$2 s).

The variation in maximum spread factor with Weber number for aqueous glycerin (75.46% glycerin) and HEC MR 250 (C = 6.0 $\times$ 10^{-9} mol/cc) solutions, and water on a Teflon substrate are graphed in Fig. 13. At low Weber number, the maximum spread factor of the polymer solution droplet is slightly more than that of aqueous glycerin. The difference between the two also increases with We. This can be attributed to the low apparent viscosity experienced by the polymeric solution droplet at higher We. The variation of the maximum spread factor with We on a glass substrate for these three test liquids is shown in Fig. 14. Here the values of $\beta_{\max}$ in each case are greater than the corresponding values of a Teflon substrate. This essentially illustrates the effect of surface wettability on the initial spreading process. Once again, the behavior of the HEC MR 250 solution droplet deviates from that of aqueous glycerin.

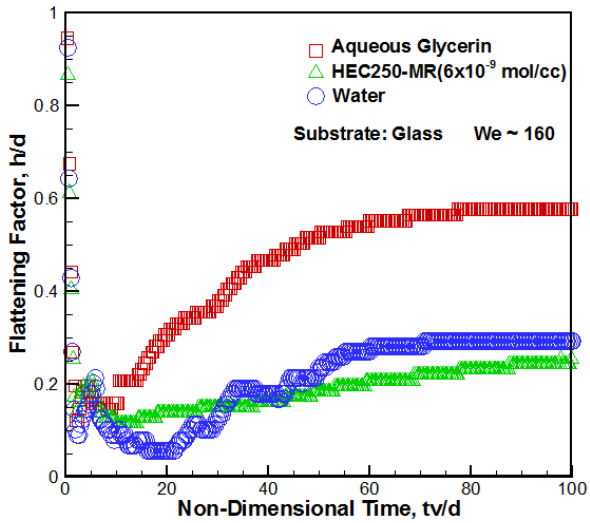

FIG. 12: Variation of flattening factor with nondimensional time. Glass substrate, We $\sim$ 160.

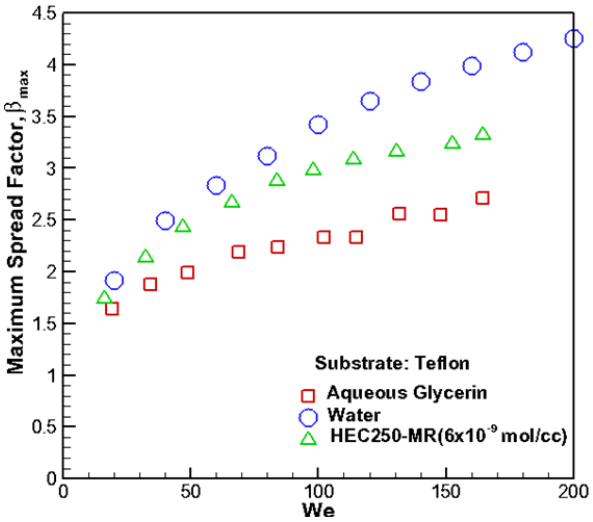

FIG. 13: Variation of the maximum spread factor (maximum uncertainty in β, $\pm$1.28%) on a Teflon substrate with Weber number.

The zero-shear-rate viscous and pseudoplastic behaviors of the aqueous polymer solutions increase significantly with the solute concentration, as seen in Fig. 4. To investigate this effect on postimpact spread dynamics, experiments were conducted with two different concentrations ($C = 6 \times 10^{-9}$ and 2.5×10^{-9} mol/cc) of HEC MR 250. While the dynamic surface tension variations of these two solutions are similar (Fig. 3), their rheological characteristics are quite different (Fig. 4). There is a large difference in both their zero-shear-rate viscosity and shear-thinning characteristics, and this affects the corresponding drop dynamics. This is seen in spread factor and flatness factor variation graphs of Figs. 15 and 16, respectively. The apparent viscosity of $C = 6 \times 10^{-9}$ mol/cc solution is always higher than that of the $C = 2.5 \times 10^{-9}$ mol/cc solution, but the difference in their apparent viscosities decreases at higher shear rates. The shear rate experienced by the droplet is highest during the initial spread, as compared to that during recoil and

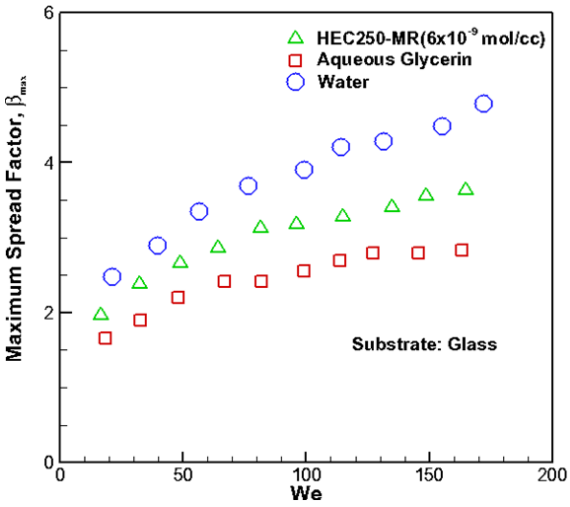

FIG. 14: Variation of the maximum spread factor (maximum uncertainty in β, $\pm 1.28\%$) on a glass substrate with Weber number.

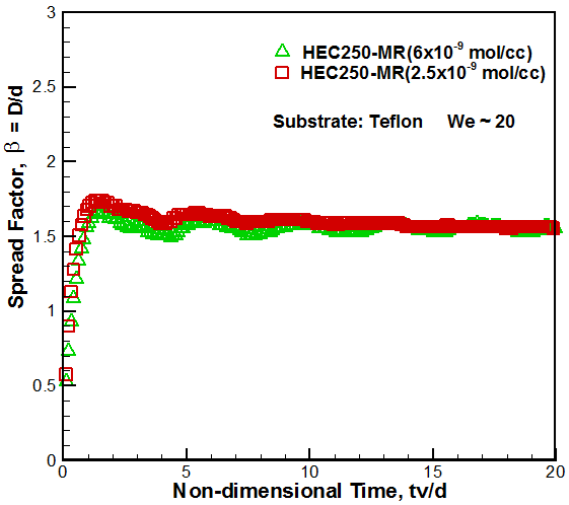

FIG. 15: Effect of polymer concentration on the variation of spread factor with nondimensional time. Teflon substrate, We $\sim$ 20.

shape oscillations. As such, during the initial spread, the difference in the apparent viscosities of the two solutions is low and their maximum spreads are nearly the same. During recoil and shape oscillations, on the other hand, the shear rates experienced are much lower. The $C = 2.5 \times 10^{-9}$ mol/cc solution droplet has a lower viscosity, compared to the higher concentration solution, and hence oscillates on the surface for a longer time period before near-equilibrium damping occurs. Contrastingly, the higher concentration ($C = 6 \times 10^{-9}$ mol/cc) solution droplet dampens rather quickly to reach equilibrium due to its much higher apparent viscosity.

4. CONCLUSIONS

The postimpact spreading and recoil behavior of millimeter-size liquid droplets of pure water, water–glycerol solution, and non-Newtonian aqueous solution of hydroxyl ethyl cellulose (HEC MR 250) on dry horizontal hydrophobic

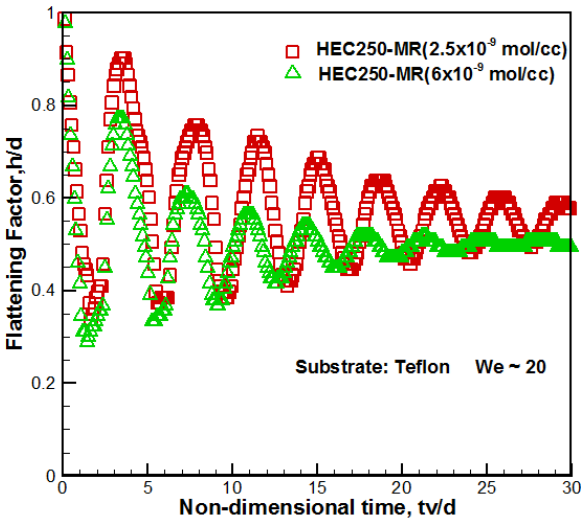

FIG. 16: Effect of polymer concentration on the variation of flattening factor with nondimensional time. Teflon substrate, We $\sim$ 20.

(Teflon) and hydrophilic (glass) substrates was investigated using high-speed, high-resolution videography. Measurements of dynamic surface tension and apparent viscosity of the polymer solutions were carried out for two different polymer concentrations. The effects of shear-thinning rheology of the polymer solution were examined by comparing its spread dynamics with that of an aqueous glycerin solution which has the same surface tension and viscosity as the equilibrium surface tension and zero-shear-rate viscosity of the polymer solution.

It is seen that the shear-rate-dependent viscosity of the polymer solution gives rise to highly complex spread–recoil dynamics. During initial spread, the shear rate experienced by the liquid is high and it behaves as a low-apparent-viscosity liquid. Moreover, because of the pseudoplasticity of the non-Newtonian polymeric solution experienced during the initial postimpact spread, the maximum spread of its droplet is higher than that for a Newtonian liquid droplet with same surface tension and identical zero-shear-rate viscosity. However, during recoil the apparent viscosity of the polymer solution is higher and it leads to slow recoil with damped shape oscillations. After a long period of time ($\sim$2 s), the droplet attains an equilibrium position with the same height and spread as its Newtonian liquid counterpart (75.46% glycerin in water solution). Furthermore, the polymer concentration determines the zero-shear-rate viscosity and shear-thinning behavior of its aqueous solution. This lends to a vastly different spread–recoil characteristics that are observed in droplets of two concentrations of HEC 250 MR solutions (C = 6 $\times$ 10^{-9} and 2.5 $\times$ 10^{-9} mol/cc). During initial spread (high shear rate), the apparent viscosity difference between the two solutions is small due to the greater pseudoplasticity in the higher concentration solution, and both have similar maximum spread. During recoil (low shear rate), however, the higher concentration solution droplet oscillations damp quickly compared to those for the lower concentration solution because of the greater viscous nature of the former.

ACKNOWLEDGMENTS

This work was supported by the National Science Foundation under Grant No. CBET-0755720. Also, the facilities provided by the Thermal-Fluids & Thermal Processing Laboratory and the experimental support work of Rupesh Bhatia and Advait Athavale are gratefully acknowledged.

REFERENCES

Asai, A., Shioya, M., Hirasawa, S., and Okazaki, T., Impact of an ink drop on paper, *J. Imaging Sci. Technol.*, vol. **37**, pp. 205–207, 1993.

Bartolo, D., Boudaoud, A., Narcy, G., and Bonn, D., Dynamics of non-Newtonian droplets, *Phys. Rev. Lett.*, vol. **99**, p. 174502, 2007.

Bergeron, V., Bonn, D., Martin, J.Y., and Vovelle, L., Controlling droplet deposition with polymer additives, *Nature*, vol. **405**, pp. 772–775, 2000.

Bhatia, R., Manglik, R. M., and Jog, M. A., Experimental evaluation of the effects of concentration and temperature on rheological properties of aqueous solutions of hydroxyethylcellulose, *Proc. of the 21st National and 10th ISHMT-ASME Heat and Mass Transfer Conf.*, Paper no. ISHMT_USA_017, IIT Madras, Chenai, India, 2011.

Bird, R. B., Armstrong, R. C., and Hassager, O., *Dynamics of Polymeric Liquids*, Vol. 1, *Fluid Mechanics*, 2nd ed., Wiley, New York, 1987.

Carre, A. and Eustache, F., Spreading kinetics of shear-thinning fluids in wetting and dewetting modes, *Langmuir*, vol. **16**, pp. 2936–2941, 2000.

Castrejón-Pita, J. R., Betton, E. S., Kubiak, K. J., Wilson, M. C., and Hutchings, I. M., The dynamics of the impact and coalescence of droplets on a solid surface, *Biomicrofluidics*, vol. **5**, no. 1, p. 14112, 2011.

Chandra, S. and Avedisian, C. T., On the collision of a droplet with a solid-surface, *Proc. R. Soc. A: Math. Phys. Sci.*, vol. **432**, pp. 13–41, 1991.

Collings, E. W., Markworth, A. J., McCoy, J. K., and Saunders, J. H., Splat-quench solidification of freely falling liquid-metal drops by impact on a planar substrate, *J. Mater. Sci.*, vol. **25**, pp. 3677–3682, 1990.

Dunleavy, J. E. and Middleman, S., Correlation of shear behavior of solutions of polyisobutylene, *J. Rheol.*, vol. **10**, no. 1, pp. 157–168, 1966.

Gatne, K. P., Jog, M. A., and Manglik, R. M., *Experimental Investigation of Droplet Impact Dynamics on Solid Surfaces, TFTPL-G1*, Thermal-Fluids and Thermal Processing Laboratory, University of Cincinnati, Cincinnati, OH, 2006.

Gatne, K. P., Manglik, R. M., and Jog, M. A., Visualization of fracture dynamics of droplet recoil on hydrophobic surface, *J. Heat Transfer*, vol. **129**, p. 931, 2007.

Gatne, K. P., Jog, M. A., and Manglik, R. M., Surfactant-induced modification of low Weber number droplet impact dynamics, *Langmuir*, vol. **25**, pp. 8122–8130, 2009.

Jones, H., Cooling, freezing, and substrate impact of droplets formed by rotary atomization, *J. Phys. D: Appl. Phys.*, vol. **4**, pp. 1657–1660, 1971.

Madejski, J., Solidification of droplets on a cold surface, *Int. J. Heat Mass Transfer*, vol. **19**, pp. 1009–1013, 1976.

Manglik, R. M., Jog, M. A., Gande, S., and Ravi, V., Damped harmonic system modeling of post-impact drop-spread dynamics on a hydrophobic surface, *Phys. Fluids*, vol. **25**, no. 8, p. 082112, 2013.

Mao, T., Kuhn, D. C. S., and Tran, H., Spread and rebound of liquid droplets upon impact on flat surfaces, *AIChE J.*, vol. **43**, pp. 2169–2179, 1997.

Moffat, R. J., Describing the uncertainties in experimental results, *Exp. Therm. Fluid Sci.*, vol. **1**, pp. 3–17, 1988.

Neogi, P. and Ybarra, R. M., The absence of a rheological effect on the spreading of small drops, *J. Chem. Phys.*, vol. **115**, pp. 7811–7813, 2001.

Nieh, S., Ybarra, R. M., and Neogi, P., Wetting kinetics of polymer solutions, Experimental observations, *Macromolecules*, vol. **29**, pp. 320–325, 1996.

Pasandideh-Fard, M., Qiao, Y. M., Chandra, S., and Mostaghimi, J., Capillary effects during droplet impact on a solid surface, *Phys. Fluids*, vol. **8**, pp. 650–658, 1996.

Rafai, S., Bonn, D., and Boudaoud, A., Spreading of non-Newtonian fluids on hydrophilic surfaces, *J. Fluid Mech.*, vol. **513**, pp. 77–85, 2004.

Ravi, V., Jog, M. A., and Manglik, R. M., Effects of interfacial and viscous properties of liquids on drop spread dynamics, ILASS2010-0142, *Proc. of 22nd Annual Meeting of the Institute of Liquid Atomization and Spray Systems*, Cincinnati, OH, 2010.

Rioboo, R., Marengo, M., and Tropea, C., Outcomes from a drop impact on solid surfaces, *Atomization Sprays*, vol. **11**, pp. 155–165, 2001.

Roisman, I. V., Rioboo, R., and Tropea, C., Normal impact of a liquid drop on a dry surface: Model for spreading and receding, *Proc. R. Soc. London, Ser. A*, vol. **458**, no. 2022, pp. 1411–1430, 2002.

Sadhal, S. S., Ayyaswamy, P. S., and Chung, J. N., *Transport Phenomena with Drops and Bubbles*, Springer, New York, 1997.

Sanjeev, A., Huzayyin, O., Gatne, K. P., Manglik, R. M., and Jog, M. A., Short time impact and cooling of water droplets impinging on hydrophobic and hydrophilic surfaces, *J. Heat Transfer*, vol. **129**, p. 080903-1, 2008.

Schonhorn, H., Frisch, H. L., and Kwei, T. K., Kinetics of wetting of surfaces by polymer melts, *J. Appl. Phys.*, vol. **37**, pp. 4967–4973, 1966.

Šikalo, Š., Marengo, M., Tropea, C., and Ganiç, E. N., Analysis of impact of droplets on horizontal surfaces, *Exp. Therm. Fluid Sci.*, vol. **25**, pp. 503–510, 2002.

Šikalo, Š. and Ganiç, E. N., Phenomena of droplet-surface interaction, *Exp. Therm. Fluid Sci.*, vol. **31**, pp. 97–110, 2006.

Ukiwe, C. and Kwok, K. Y., On the maximum spreading diameter of impacting droplets on well-prepared solid surfaces, *Langmuir*, vol. **21**, pp. 666–673, 2005.

Yang, X., Chhasatia, V.H., Shah, J., and Sun, Y., Coalescence, evaporation and particle deposition of consecutively printed colloidal drops, *Soft Matter*, vol. **8**, pp. 9205–9213, 2012.

Yang, X., Chhasatia, V. H., and Sun, Y., Oscillation and recoil of single and consecutively printed drops, *Langmuir*, vol. **29**, pp. 2185–2192, 2013.

Yarin, A. L., Drop impact dynamics: Splashing, spreading, receding, bouncing..., *Annu. Rev. Fluid Mech.*, vol. **38**, pp. 159–192, 2006.